communications earth & environment

ARTICLE

https://doi.org/10.1038/s43247-023-00835-0 OPEN

Autumn canopy senescence has slowed down with global warming since the 1980s in the Northern Hemisphere

Yichen Zhang [1], Songbai Hong[1], Qiang Liu [2✉], Chris Huntingford [3], Josep Peñuelas [4,5], Sergio Rossi[6], Ranga B. Myneni[7] & Shilong Piao [1,8✉]

Climate change strongly impact vegetation phenology, with considerable potential to alter land-atmosphere carbon dioxide exchange and terrestrial carbon cycle. In contrast to well-studied spring leaf-out, the timing and magnitude of autumn senescence remains poorly understood. Here, we use monthly decreases in Normalized Difference Vegetation Index satellite retrievals and their trends to surrogate the speed of autumn senescence during 1982–2018 in the Northern Hemisphere (>30°N). We find that climate warming accelerated senescence in July, but this influence usually reversed in later summer and early autumn. Interestingly, summer greening causes canopy senescence to appear later compared to an advancing trend after eliminating the greening effect. This finding suggests that summer canopy greening may counteract the intrinsic changes in autumnal leaf senescence. Our analysis of autumn vegetation behavior provides reliable guidance for developing and parameterizing land surface models that contain an interactive dynamic vegetation module for placement in coupled Earth System Models.

[1] Sino-French Institute for Earth System Science, College of Urban and Environmental Sciences, Peking University, Beijing 100871, China. [2] PLECO (Plants and Ecosystems), Department of Biology, University of Antwerp, Universiteitsplein 1, 2610 Wilrijk, Belgium. [3] UK Centre for Ecology and Hydrology, Wallingford, Oxfordshire OX10 8BB, UK. [4] CREAF, Cerdanyola del Valles, Barcelona 08193 Catalonia, Spain. [5] CSIC, Global Ecology Unit CREAF-CSIC-UAB, Bellaterra, Barcelona 08193 Catalonia, Spain. [6] Laboratoire sur les écosystèmes terrestres boréaux Département des Sciences Fondamentales, Université du Québec à Chicoutimi, Chicoutimi, Quebec G7H 2B1, Canada. [7] Department of Earth and Environment, Boston University, 685 Commonwealth Avenue, Boston, MA US-02215, USA. [8] State Key Laboratory of Tibetan Plateau Earth System, Resources and Environment, Institute of Tibetan Plateau Research, Chinese Academy of Sciences, Beijing 100085, China. ✉email: qiang.liu@uantwerpen.be; slpiao@pku.edu.cn

Autumnal senescence is a critical component of the seasonal evolution of terrestrial ecosystems, which regulates the length of the growing season and terrestrial carbon uptake[1,2]. Yet, such event and its response to changing climate is not well represented in most Earth System Models (ESMs)[3]. Impact of climate change on the trends of autumn senescence as well as its role in terrestrial carbon, water, nutrient cycling, fitness, and distribution of tree species have been reported over the past decades[1,2,4–9]. Many of them focused on the timing of specific phenophase, e.g., leaf coloring and abscission[1]. However, the process of autumn senescence consists of a series of complex metabolic events such as macromolecule degradation, decreased photosynthesis, and most importantly, nutrient reabsorption[10–12]. These events are co-dominated by plant internal conditions (e.g., metabolic adjustments, genetic expressions), near-surface meteorological factors (e.g., temperature, solar radiation and wind), water availability and their interactions[12–14]. Despite the complex climatic responses of autumn phenology, it remains unclear, however, which stage of the senescence process contributes more to changes in the timing of end of the growing season (EOS). Moreover, previous studies pay too much attention to individual phenophases (e.g., EOS), which may conceal other components of the senescence process, such as the variations in the environmental regulations during the multiple stages of the autumn senescence process[15]. These gaps in knowledge would leave the reliable modelling of autumn senescence in doubt[16], and finally hamper the ability of ESMs to simulate vegetation dynamics under future climatic scenarios[17,18].

Here, we provide a timely assessment of autumn senescence speed through the monthly decreases in NDVI (ΔNDVI, see schematic representation in Fig. 1), which is also critical for the extraction of EOS. We first investigate the regulations of climatic factors (temperature, soil moisture, insolation i.e., downward shortwave radiation, and windspeed) on the speed of autumn senescence (i.e., the interannual trends in ΔNDVI). Given that such behavior may be confounded by rising CO_2-induced summer canopy greening (i.e., uptrends in annual maximum NDVI, $NDVI_{max}$), we additionally calculated the relative decrease of NDVI ($\delta NDVI = \Delta NDVI/NDVI_{max}$) as a surrogate for ΔNDVI (see definitions in Supplementary Table 1). Then, we quantified the effects of increasing $NDVI_{max}$ (i.e., canopy greening) on ΔNDVI, and consequently, the extracted EOS. Together with this analysis, we discussed the implications of our study on benchmarking phenological modules for future generations of Earth System Models (ESMs).

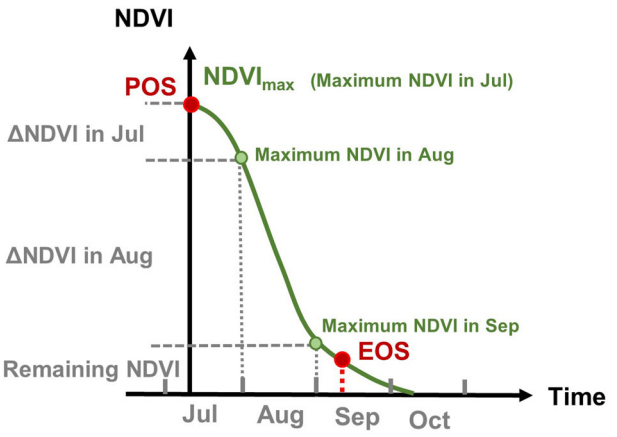

Fig. 1 Schematic representation of NDVI variations during the autumn senescence process. In this study, autumn senescence starts at Peak Of Season (POS) when NDVI reaches its annual maximum ($NDVI_{max}$), and ends at the End Of Season (EOS). The monthly decrease in NDVI (ΔNDVI) is estimated as the NDVI difference between the current and the following months (in positive values), and the remaining NDVI is the NDVI left in the EOS month (in positive values). The sum of monthly ΔNDVI and the remaining NDVI is therefore equal to $NDVI_{max}$. Detailed definitions of these items can be found in Supplementary Table 1.

Results and Discussion

Changes in the speed of autumn senescence. Across the Northern Hemisphere (>30°N, NH, thereafter), divergent trends in ΔNDVI can be discerned among the senescence months, with larger increasing trend found in July ($1.8 \times 10^{-4}\,yr^{-1}$) and September ($2.1 \times 10^{-4}\,yr^{-1}$), whereas decreasing trends were found for August ($-3.7 \times 10^{-5}\,yr^{-1}$) and October ($-1.7 \times 10^{-4}\,yr^{-1}$; Fig. 2a). There is also an increasing trend in ΔNDVI for the entire senescence period (July to October, JASO) (Fig. 2b), although noting this may be expected due to rising $NDVI_{max}$ under planetary greening (Fig. 2c). Dramatic regional variations, however, existed in ΔNDVI trends across the NH (Fig. 2d–i). Specifically, we found ΔNDVI increased in northwestern North America in July, which dominated the acceleration of autumnal senescence during the senescence period (Fig. 2d, h). In contrast, negative ΔNDVI trends were mainly distributed in northeastern North America and eastern Eurasia during August, which contributed to a slowing of the speed of autumn senescence (Fig. 2e, h). In September, contrasting changes in ΔNDVI were observed between the high and middle latitudes of Eurasia (Fig. 2f), resulting in opposite trends in the speed of autumn senescence (e.g., acceleration in middle Eurasia but deceleration in higher latitudes) (Fig. 2h). We also found that the speed of autumn senescence slowed down in the west and east of North America in October, when vegetation was already in dormant phase across most high latitudes (Fig. 2g).

Overall, ΔNDVI over the entire senescence period increased in 53.1% of the NH (significant in 17.9%, Fig. 2h), implying an overall acceleration of autumn senescence would occur in these areas. Although acceleration of senescence was found in more than half of the NH, the remaining NDVI (NDVI left in the month of EOS, see definition in Fig. 1 and Supplementary Table 1) still exhibited positive trends in 69.4% of the NH (Fig. 2i). These findings are anticipated due mainly to the apparent summer greening (i.e., a prevalent increase in $NDVI_{max}$, Supplementary Fig. 1). Indeed, when averaged across NH, $NDVI_{max}$ increased significantly at a rate of $8.4 \times 10^{-4}\,yr^{-1}$ ($p < 0.001$) during the senescence period (Fig. 2c). Meanwhile, ΔNDVI over JASO general increased, but its magnitude ($2.1 \times 10^{-4}\,yr^{-1}$, $p > 0.05$) is weaker than that of $NDVI_{max}$. As a result, the remaining NDVI had an overall positive trend ($6.3 \times 10^{-4}\,yr^{-1}$, $p < 0.001$). Our analysis, therefore, reveals that changes in the speed of autumn senescence (ΔNDVI) and the peak greenness ($NDVI_{max}$) can affect vegetation greenness at the later stage of the growing season.

Climatic regulation on the speed of autumn senescence. To investigate the climatic regulations on the speed of autumn senescence, we conducted partial correlation analyses to isolate the influence of insolation, wind speed, soil moisture, and temperature (Supplementary Fig. 2). The factor with the strongest partial correlation with ΔNDVI was defined as the dominant driver of autumn senescence (see Methods). Again, the dominant factors that accelerate or slow down the speed of autumn senescence were heterogeneous and discernible in their patterns over the NH (Supplementary Fig. 3).

Our noted strong spatial variations in ΔNDVI trends may be explained by the divergent biological responses of plants to

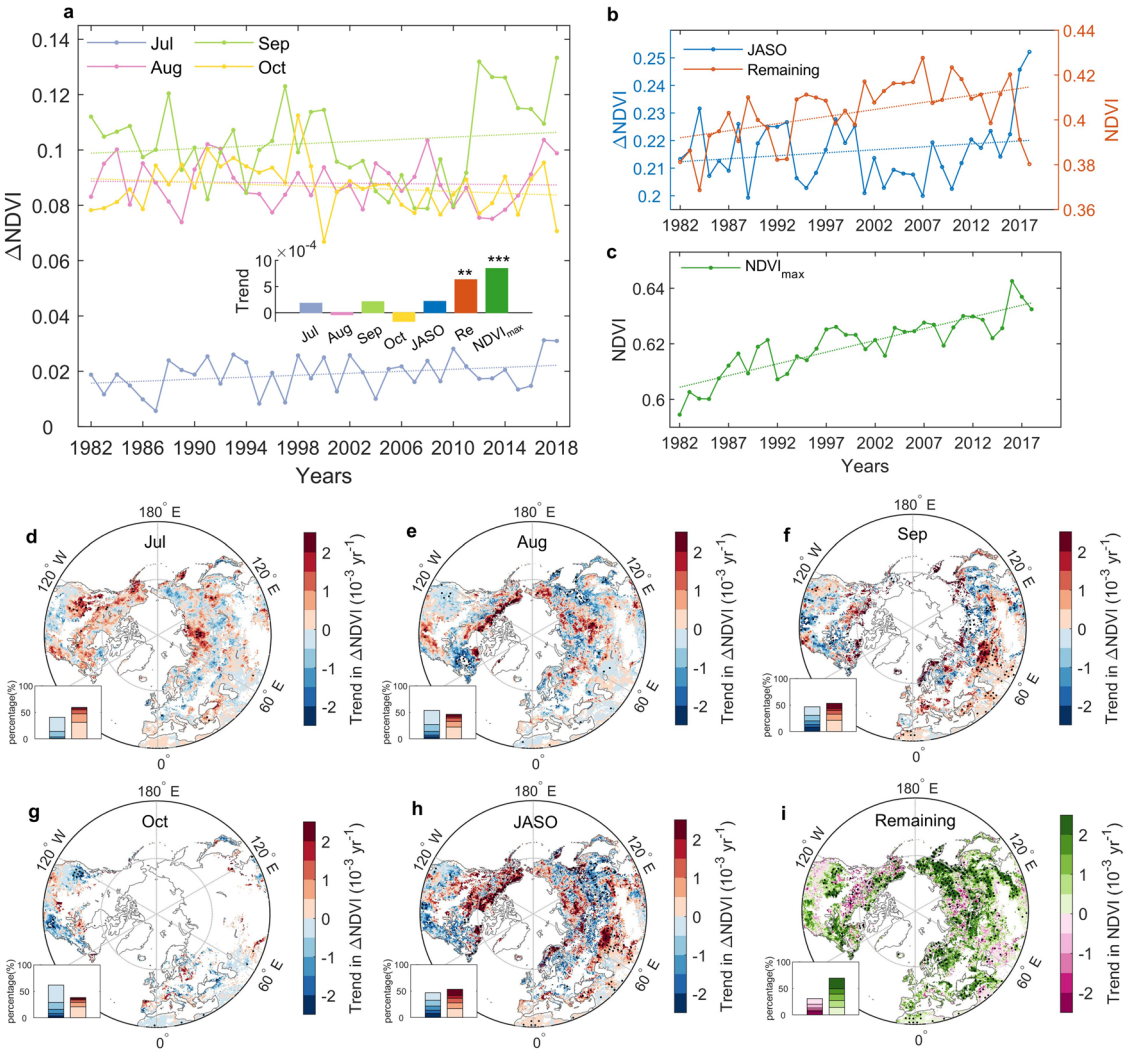

Fig. 2 Trends in ΔNDVI over individual months and the entire senescence period from 1982 to 2018. a Temporal trends of ΔNDVI for senescence months in the Northern Hemisphere (NH) (recalling that a positive value of ΔNDVI corresponds to a decrease in NDVI). **b** Temporal trends of ΔNDVI over the senescence period (from July to October, JASO) and remaining NDVI at the end of the autumn senescence. **c** Temporal trends of the annual maximum NDVI ($NDVI_{max}$). The bars inserted in **a** indicate trends in ΔNDVI for each month, the whole senescence period, and the remaining NDVI. **d**–**i** Spatial patterns of ΔNDVI trends during 1982–2018 for senescence months (**d**–**g**), the entire senescence period (**h**), and remaining NDVI (**i**). Black dots in **d**–**i** indicate significant trends at 0.05 level, while the inserted stacked bars indicate the frequency distributions of ΔNDVI trends.

climate change across different climatic regions. In fact, climatic regulations on ΔNDVI trends (higher values indicate a greater senescence speed, Fig. 1) were mainly associated with local hydrothermal conditions (Fig. 3). At the beginning of the autumn senescence period (that is, July), ΔNDVI correlated positively with temperature, but negatively with soil moisture in colder (mean annual temperature, MAT < 5 °C) and relatively drier (mean annual precipitation, MAP < 500 mm) regions (Fig. 3a, f). This finding indicated a possible acceleration of senescence caused by warming, because climatic warming may in turn lead to severe soil water deficits. Meanwhile, insolation was identified as a major promotor of the speed of autumn senescence in 33.2% of NH (Fig. 3k). Interestingly, the overall temperature effects on ΔNDVI shifted from positive (July) to negative (August, September, and October) as autumn senescence progresses. The negative temperature dominance on ΔNDVI trends over the NH increased from ~31% (August and September, Fig. 3l, m) to 46.9% (October, Fig. 3n). These results imply that a warming climate could accelerate autumn senescence in earlier stages of the senescence period, probably due to the detrimental summer extreme temperatures. On the other hand, it might significantly slow down the speed of senescence in its later stages by prolonging the exposure of vegetation to favorable summer climate.

Unlike such reversal of temperature regulation on the speed of autumn senescence, the effects of insolation, soil moisture and windspeed remained almost consistent along the senescence period. To be specific, insolation was identified as the positive dominant factor of ΔNDVI, particularly over the warmer regions (MAT > −5 °C) and the lower latitudes (Fig. 3). Because the increasing insolation might raise the risk of leaf photo-oxidative damage, which could promote the progress of leaf senescence[19]. As for soil moisture and wind speed, their influence is only apparent in a few sporadic areas.

While for the remaining NDVI (higher values indicate slower senescence speed, Fig. 1), it was generally positively related to temperature and insolation, but negatively related to wind speed (Fig. 3e, j, o). The positive temperature effect was prevalently observed over the NH (Supplementary Figs. 2x, 3f), which confirmed again that warming climate contribute to slow down

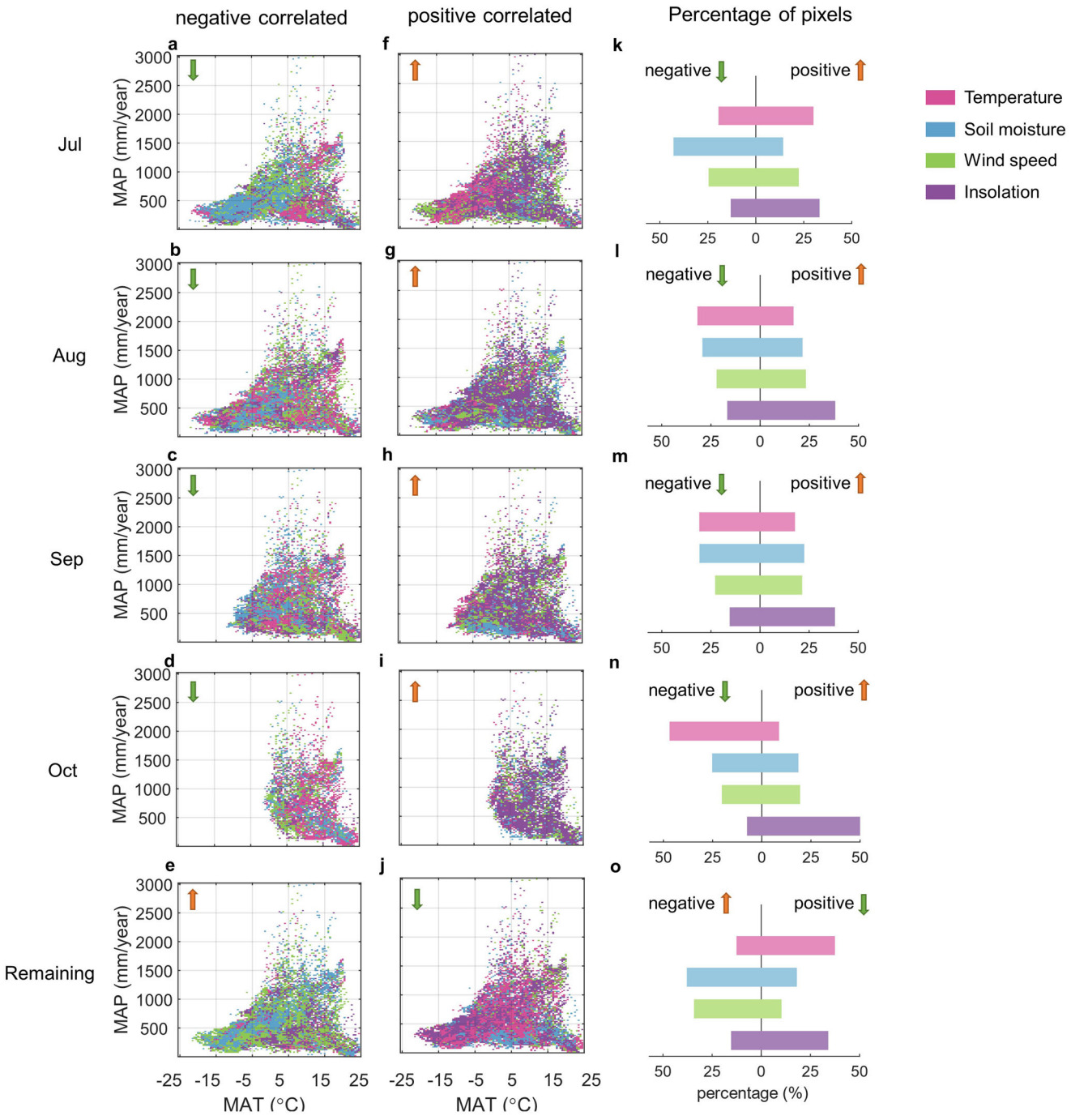

Fig. 3 The dominant climatic factors of the trends in ΔNDVI and the remaining NDVI. a–e The distribution of dominant climatic factors was negatively correlated with ΔNDVI for the senescence months (**a**–**d**) and the remaining NDVI (**e**) in the climate space. **f–j** The distribution of dominant climatic factors was positively correlated with ΔNDVI for the senescence months (**f**–**i**) and the remaining NDVI (**j**) in the climate space. Each climate bin was defined by 0.5 °C intervals of mean annual temperature (MAT) and 20 mm intervals of mean annual precipitation (MAP). The factor that appeared most frequently for each bin was presented in these figures. **k–o** The percentages of pixels occupied by dominant climatic factors, which positively (left bars, add to 100%) and negatively (right bars, add to 100%) correlated with ΔNDVI for senescence months (**k**–**n**) and the remaining NDVI (**o**). Note that the positive correlation with ΔNDVI or the negative correlation with the remaining NDVI indicates that this factor can accelerate the speed of autumn senescence, and vice versa.

the speed of senescence in late autumn. Followed by insolation, its positive and dominant effects on the remaining NDVI were mainly distributed in North Siberia and North America (with MAT < 0 °C) (Supplementary Figs. 2e, 3e), indicating the negative light regulation on leaf senescence was stronger than that of warming for these regions[20]. We also found that the wind speed exerted negative controls on the remaining NDVI in 34.3% of NH (Fig. 3e, o) through its role in promoting leaf abscission and intensifying drought stress by increasing evapotranspiration[7]. The influence of soil moisture expressed a contrasting regional difference (Supplementary Fig. 2q). More specifically, in terms of inland Eurasia and North America, the remaining NDVI was positively regulated by soil moisture (Supplementary Fig. 2q), indicating that increases in soil moisture can slow down the speed

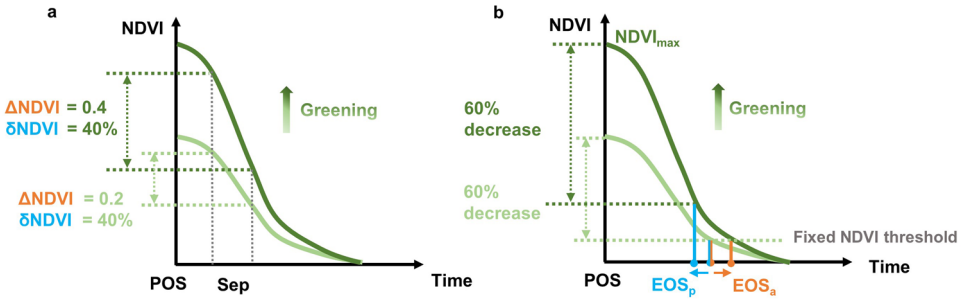

Fig. 4 Schematic representation of the influence of greening on the speed of monthly senescence and the detection of EOS. a For each senescence month, monthly senescence is proxied by the decrease in NDVI (ΔNDVI) or percentage of decrease in NDVI relative to $NDVI_{max}$ (δNDVI = ΔNDVI/$NDVI_{max}$). Peak of season (POS) greening would lead to an apparent increase in ΔNDVI even if δNDVI stays invariant. **b** In correspondence to ΔNDVI and δNDVI, end of season can be determined by fixed NDVI thresholds (EOS_a) or fixed percentage of $NDVI_{max}$ (EOS_p). If $NDVI_{max}$ were kept unchanged, these two methods would deliver the same EOS, whereas increases in $NDVI_{max}$ would results to a later EOS_a than EOS_p.

of autumn senescence in these water-limited ecosystems. However, in high-latitude Siberia (>50°N), soil moisture was negatively correlated with the remaining NDVI (Supplementary Fig. 2q), mainly due to the anoxia conditions under high soil moisture[21] and limited nutrient availability in these regions of permafrost[6].

The effect of summer greening on the extraction of autumn phenology. Parallel to climate change, the observed summer greening (that is, an increase of $8.4 \times 10^{-4}\,yr^{-1}$ in $NDVI_{max}$, $p < 0.001$, Fig. 2c) could modulate the extracted autumn phenology and its temporal trend. We hypothesize that, accompanied with summer greening, the increasing mature leaves in the peak season would contribute to an increasing trend in ΔNDVI, thus creating an illusion of faster senescence (Fig. 4a). Such effect could be greatly reduced by replacing monthly senescence (ΔNDVI) with the relative decrease in NDVI (δNDVI = ΔNDVI/$NDVI_{max}$). Summer greening, in a similar way, would contribute to delayed EOS calculated from fixed NDVI thresholds (EOS_a) than that from fixed percentage of $NDVI_{max}$ (EOS_p), implying the influence of changing $NDVI_{max}$ in EOS detection (Fig. 4b, also see definitions in Supplementary Table. 1).

Notably, trends in δNDVI generally presented similar spatial patterns as that of ΔNDVI in each of the senescence months (Supplementary Fig. 4a–e). After separating the contribution of trends in $NDVI_{max}$ and δNDVI to trends in ΔNDVI (Supplementary Fig. 5a–e, see Methods), we found that the increase in $NDVI_{max}$ accounted for ~40% of ΔNDVI trends in NDVI for parts of Siberia and central Eurasia in August and September (Supplementary Fig. 5b, c). Despite this, the overall contribution of $NDVI_{max}$ to ΔNDVI trends was marginal for other regions and periods (e.g., only 1.7, 5.9, 5.0 and 2.6% for Jul, Aug, Sep and Oct, respectively). Such influence was confirmed by the relatively small portion of significant correlations between trends in $NDVI_{max}$ and ΔNDVI for these months (Supplementary Fig. 6a–d). Besides, similar spatial patterns of dominant climatic factors were also observed in δNDVI, further indicating their tight connection (Supplementary Fig. 3).

We also found that the influence of increasing $NDVI_{max}$ on trends of the remaining NDVI was apparent (36.7% on average, Supplementary Fig. 5f), which was in line with the widespread significant correlations between trends in $NDVI_{max}$ and the remaining NDVI over the NH (Supplementary Fig. 6f). This leads to higher fractions of positive trend areas for the remaining NDVI (69.4% with 30.1% significant, Fig. 2i) than its percentage-based counterpart (55.3% with 14.7% significant, Supplementary Fig. 4f). Obviously, the impact of conspicuous summer greening on the remaining NDVI may have cascaded effects on the extraction of EOS.

We therefore further compared the temporal trends of EOS_a and EOS_p (definitions in Fig. 4b, also see definitions in Supplementary Table. 1) during the period 1982–2018. Across the NH, we found areas occupied with delayed EOS_a (60.2%, significant in 22.2%, Fig. 5a) exceeds that of EOS_p (51.1%, significant in 15.1%, Fig. 5b). As a result, an overall delayed trend of EOS_a (0.6 days dec^{-1}) but advanced EOS_p (−0.4 days dec^{-1}) trend was presented in NH (Fig. 5a–c). This divergence summed up to 1.0 days dec^{-1} $NDVI_{max}$-induced delay in EOS_a. Given that such an advance in autumn senescence was supported by a meta-analysis based on field observations[22], we reckon that EOS_p may be a better indicator of autumnal leaf phenology, which captures the physiological changes of plants. EOS_a, carrying the additional effect of $NDVI_{max}$, my instead, serve as a better indicator for canopy greenness browning. Our results thus infer that the increase in the number of mature leaves in the canopy under summer greening may counteract the intrinsic changes in autumnal leaf senescence.

Among the studied plant functional types (PFTs), we also observed clear mismatch between trends in EOS_a and EOS_p (Fig. 5d). In line with the NH average (a combination of all PFTs), we found the opposite contributions of $NDVI_{max}$ (delay) and EOS_p (advance) to EOS_a trends in grasslands, savannas and shrublands in boreal and arctic regions. However, the delaying effect of summer greening could hardly compensate for the large advancement in EOS_p, as these ecosystems generally locate in resource-limited areas (Supplementary Fig. 7). Growth enhancement (greening) during the earlier season may prematurely consume water and nitrogen, which would in turn speed up the progress of vegetation senescence and cause earlier end of growing season[23–25]. Indeed, the largest advancement in EOS_p was observed in grasslands of central Eurasia, which were characterized with severe water limitations and significant vegetation greening (Supplementary Fig. 1).

The observed delay in EOS_p for the woody species could be ascribed to the higher resource availability in their relatively wetter and fertile habitants, and their ability to accumulate large nutrient and carbohydrate reserves in autumn[26,27]. The increase in $NDVI_{max}$ contribute to later EOS_a than EOS_p, albeit varied across these PFTs (Fig. 5d). We quantified the contribution of increasing $NDVI_{max}$ to the delayed EOS_a through the residue proportion of trends after subtracting EOS_p from EOS_a (i.e., the proportion of orange bars within the transparent purple bars, last section of methods). As a result, the increase in $NDVI_{max}$ contributed to more than half of the delay in EOS_a for woody savannas (69.2%) and temperate shrublands (88.5%). However,

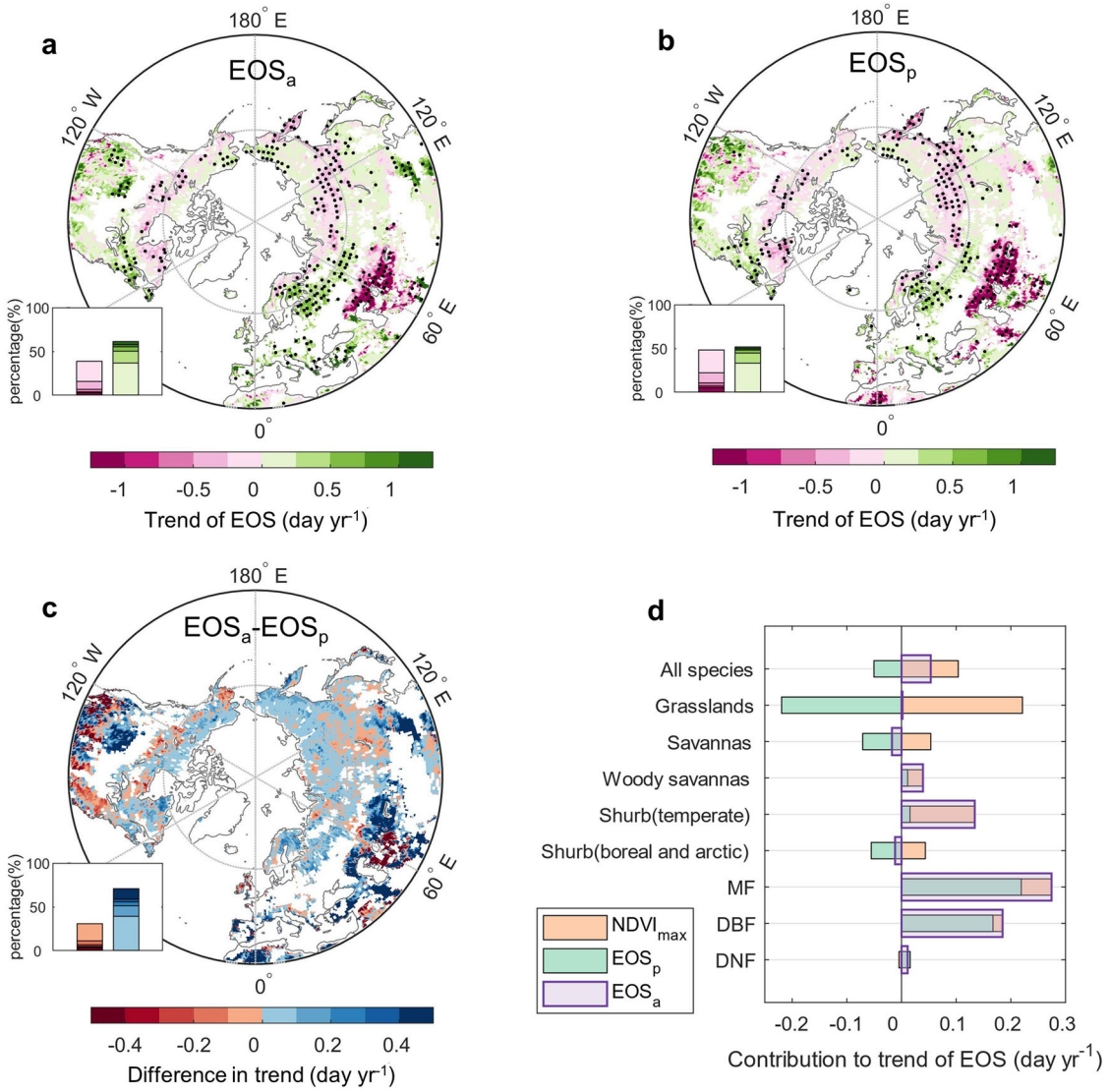

Fig. 5 Mismatch between end-of-season (EOS) determined by fixed thresholds of NDVI (EOS_a) and fixed percentages of $NDVI_{max}$ (EOS_p). a, **b** Spatial patterns of trends in EOS_a and EOS_p in 1982–2018. Black dots indicate a significant trend at the 0.05 level. The stacked inserted bars indicate the frequency distributions of trends in EOS_a and EOS_p. **c** Difference between trends in EOS_a and EOS_p (trends in EOS_a minus trends in EOS_p). **d** Contribution of trends in EOS_p (green bars) and $NDVI_{max}$ (i.e., EOS_a-EOS_p, orange bars) to trends in EOS_a (purple bars) for different vegetation types (see Methods). MF mixed forests, DBF deciduous broadleaf forests, DNF deciduous needleleaf forests.

such influence is minor in forests, contributing to 20.3% and 9.5% in mixed forests and deciduous broadleaf forests, respectively. On the contrary, the decrease in $NDVI_{max}$ in deciduous needleleaf forests advanced EOS_a by 29.3%, comparing to EOS_p.

Remarkably, $NDVI_{max}$-induced divergence between EOS_a and EOS_p trends exerted strong controls on their responses to climate change (Supplementary Figs. 2, 8). Despite the observed clear positive temperature dominance for EOS_a and EOS_p (Supplementary Fig. 3f, r), the difference in the sensitivities of EOS_a and EOS_p to temperature was examined (e.g., EOS_a (γ_a) and EOS_p (γ_p), see Methods). The partial least squares regressions analysis suggested that both EOS_a and EOS_p had positive temperature sensitivities in most areas, while negative sensitivities were concentrated in xeric grasslands of central Eurasia and USA (Supplementary Fig. 9a, b). Note that EOS_a presented larger temperature sensitivities than EOS_p in 69.5% of northern areas, e.g., γ_a (2.1 days $°C^{-1}$) was more than 50% higher than γ_p (1.3 days $°C^{-1}$) when averaged over the NH (Supplementary Fig. 9c), due mainly to the additional $NDVI_{max}$ greening trend carried by EOS_a. Indeed, the prominent differences between γ_a and γ_p were discovered in grasslands and temperate shrublands (Supplementary Fig. 9d), where EOS_a trends were predominantly contributed by changes in $NDVI_{max}$ (Fig. 5d).

Implications for model benchmarking. The mismatch between phenology metrics based on absolute (ΔNDVI, EOS_a) and relative (δNDVI, EOS_p) changes in NDVI indicates the considerable effect of summer greening on the extraction of autumn phenology. In other word, the increase in the number of mature leaves in canopy under summer greening might confound the actual changes in the timing of leaf senescence. Such an effect is most clearly shown by the mismatch between EOS_a and EOS_p. EOS_a, derived from fixed thresholds of NDVI, is a direct reflection of drop in canopy greenness, with a delayed trend in EOS_a indicating the prolonged canopy browning process. EOS_p, derived from fixed percentages of $NDVI_{max}$, instead, better captures senescence of leaves under the overall changes in canopy greenness. As shown in our results, the widely observed

global greening (Supplementary Fig. 1) in this study and previous studies[28,29], has, indeed, counteracted the intrinsic advance of leaf senescence by an apparent delay in canopy browning. Despite that these two metrics may represent phenology at different ecological levels (e.g., leaf vs. canopy), leaf phenology is more closely related to the time when plants enter winter dormancy and is a key regulator of vegetation dynamics and terrestrial carbon sequestration[2]. The absence of eliminating the summer greening effect in the extraction of autumn phenology (i.e., threshold-based methods: EOS_a) may introduce bias to our understanding of the leaf senescence process and consequently, the vegetation-climate interactions and the terrestrial carbon cycle. Since the timing of leaf senescence is crucial for reconstructing historical plant carbon uptake and predicting its future changes in Earth system models, it is essential to update phenology modules embedded in state-of-the-art land surface schemes using accurate representations of these processes. This will enable a better simulation of the terrestrial carbon cycle[30,31].

However, leaf senescence so far is one of the most difficult processes to be parameterized in terrestrial ecosystem models, which is restricted by our incomplete understandings of its complex mechanisms. To our knowledge, DGVMs coupled with land surface models generally determine the onset of plant dormancy by tracking the thresholds of modelled or prescribed leaf area index[30]. For example, in the ORCHIDEE model, it is defined as the date when the modelled leaf area index (LAI) drops below 0.2[32]. Evidence from our study suggests that fixed thresholds, however, may not accurately reproduce the timings of autumn leaf phenology when the summer greening effect is not thoroughly considered. Other models, for example, the Ecosystem Demography model version 2 (ED2), used the prescribed satellite-derived EOS estimates to parameterize the date of leaf drop during the year[33]. In this case, an accurate estimation of EOS, especially taking the effect of summer greening into consideration, is of great importance for accurate model parameterizations. Moreover, a large body of models simulates the timing of leaf shed by a function of air temperature and (or) day length[34–36]. Although these models directly simulate leaf phenology, caution is still needed for benchmarking models against satellite-derived results, since phenology based on absolute changes in vegetation greenness may be not sufficient to characterize the trajectories of leaf senescence.

We also found that EOS_a, carrying the additional greening trend at POS, generally exhibits higher temperature sensitivities than EOS_p. This discrepancy was in support of findings in Zhang et al. (2020), who reported that the response of greenness-based phenology to climate change was greater than that of photosynthesis-based phenology. Therefore, if the apparent sensitivity of satellite-based leaf phenology (with the absence of a summer greening effect in the extraction of phenology) is used to parameterize leaf behavior in DGVMs, the future carbon sink potential of terrestrial ecosystems might be overestimated.

Our study provides a novel angle on the speed of autumn senescence and its response to climate change over the NH. We find that warming climate accelerates senescence in July, but this influence usually reversed in later summer and early autumn. Insolation generally accelerates senescence across the entire senescence period. Our analysis also verifies a summer greening (increase in $NDVI_{max}$)-induced delay in EOS, as canopy greening may counteract the intrinsic changes in leaf phenology, and lead to higher temperature sensitivities for EOS carrying the additionally greening trend. Global warming and increasing atmospheric CO_2 have been reported to continually contribute to earth greening, especially in NH[28,29]. Our analysis thus allows us to reconsider the linkage between changes in apparent canopy greenness and changes in intrinsic leaf physiology, which could provide an important benchmark for those developing DGVMs for use in ESMs.

Methods

Datasets. In this study, NDVI during the 1982–2018 period was extracted from the third-generation product of NASA's Global Inventory Modeling and Mapping Studies (GIMMS) group[37]. Various issues, such as orbital drift, calibration, viewing geometry and volcanic aerosols, have been corrected in this product[38]. This dataset consists of fortnightly NDVI observations at a spatial resolution of 0.083° (~8 km). The monthly NDVI data was estimated through the maximum composition of each month's two records. In this analysis, we screened out pixels dominated by cropland and evergreen forests (inferred from the MODIS Landcover Product, MCD12C1, IGBP classification)[39], because their seasonal cycles are unclear. Consistent with the NDVI time span, the monthly mean 2-m surface temperature was derived from CRU.TS.4.05 with 0.5° spatial resolution[40]. Monthly insolation was extracted and summed from CRU-JRA v2.2 with 0.5° spatial and 6-h temporal resolution[41]. The monthly surface soil moisture was acquired from the C3S dataset provided by the European Center for Medium-Range Weather Forecasts (ECMWF) with a 0.25° spatial resolution, which was then interpolated to 0.5° × 0.5°. The monthly wind speed was obtained from the ERA5 reanalysis data at a spatial resolution of 0.25° [42] and was interpolated to 0.5° × 0.5°.

Phenology extraction methods. Our study was conducted across north of 30°N (excluding the subtropical regions), where plants have clear seasonal variations and are capable to extract phenological metrics. The Autumn senescence period is defined as the time window between POS (Supplementary Fig. 10) and EOS (Supplementary Fig. 11). The decrease in NDVI (ΔNDVI) during the entire senescence period was defined as the difference in NDVI between POS month and EOS month. Similarly, the monthly ΔNDVI was the NDVI difference between the current and the following month. The remaining NDVI i.e., NDVI at EOS month, refers to the remaining greenness in the final stage of autumn senescence. For the minor regions with later POS (e.g., later than July, only 6.2% of the study area), the calculation of ΔNDVI also starts from POS month, NDVI data prior to the POS month was excluded from the analysis.

Besides monthly senescence, we further obtained threshold-based EOS (EOS_a). To avoid the influence of potential snow cover on EOS extraction, we first used the spline function to interpolate the monthly temperature to a daily basis, and then obtained the boundary of the thermal growing season by a sequence of five days below 0 °C. Before EOS extraction, NDVI pixels outside this thermal growing season were replaced by that of the temporally nearest snow-free date. We than determined EOS_a according to the following steps (Polyfit-Maximum method[43]; Supplementary Fig. 12): (1) calculate the averaged NDVI curves during the past 37-year (1982–2018), (2) estimate the rates of changes in the average NDVI curves as: $NDVI_{ratio}(t)=[NDVI(t+1)-NDVI(t)]/NDVI(t)$, (3) determine the time T when the minimum $NDVI_{ratio}$ occurred, (4) use the NDVI at time T (i.e., NDVI(T)) as the threshold for EOS_a extraction, (5) apply the threshold to determine EOS_a for each year. The Polyfit-maximum method have been successfully used in many of previous phenological studies[44–46], and its outcomes are comparable with other commonly used methods[6]. The priorly determined NDVI threshold also gives us the chance to correspondently obtain a percentage-based threshold, which is then used for further analysis (see detection of EOS_p in next paragraph).

The extraction of ΔNDVI and EOS_a is probably confounded by global greening, especially in the context of the prominent increase in $NDVI_{max}$ (i.e., the effect of summer canopy greening, Fig. 4 and Supplementary Fig. 1). To reduce such an impact, we employed another method based on the percentage of $NDVI_{max}$. During each month and the entire senescence period, we calculated the percentage of decrease in NDVI compared to the peak season NDVI as $\delta NDVI = \Delta NDVI / NDVI_{max}$. Similarly, the percentage of remaining NDVI relative to $NDVI_{max}$ was calculated as the division between the remaining NDVI and $NDVI_{max}$. The percentage-based EOS (EOS_p) was extracted from almost the same steps as EOS_a, except that the percentage of NDVI(T) relative to $NDVI_{max}$ ($NDVI(T)/NDVI_{max}$) were used as thresholds to detect yearly EOS_P (step 4, Supplementary Fig. 12). The differences in ΔNDVI and δNDVI, and EOS_a and EOS_p gives us chance to investigate the effect of $NDVI_{max}$ on autumn phenology detection (see last section of methods).

Climatic regulations on the process of autumn senescence. Benefiting from previous studies, we examined the effects of four climatic factors i.e., insolation, wind speed, soil moisture, and temperature on the leaf senescence process[6,7,14,47]. Note that we did not take precipitation into consideration, due mainly to the following aspects: (1) Soil moisture is extensively correlated with precipitation in the study area (Supplementary Fig. 13) and (2) soil moisture is more closely and directly related to plant water uptake than precipitation[5,48]. The lagged effect of climate on vegetation dynamics was also considered for each of the phenological matrices (ΔNDVI, δNDVI, EOS_a and EOS_p) following previous studies[6,8,15]. Firstly, simple correlations were used to determine the preseason length of each climatic factors, which was defined as the period when the mean value of factors having the largest absolute simple correlation with phenological metrics (Supplementary Figs. 14, 15). The preseason length ranged from the month of phenology metrices to its preceding 3 months, with a monthly time step. The preseason was defined for each of the four phenological metrics and climatic variables. We then performed partial correlation analysis between each of the phenological metrices and climatic factors during the preseason (Supplementary Figs. 2, 8). It enables us

to explore the relationship between plant phenology and single climatic factor while eliminating the effects of the remaining factors. The climatic factor with the largest positive (lowest negative) partial correlation coefficient was defined as the positive (negative) dominant factor (Supplementary Fig. 3).

Temperature sensitivity of EOS. Our partial correlation analysis suggested distinct temperature dominances on EOS_a and EOS_p, while similar patterns were not clear for ΔNDVI and δNDVI. We then performed a partial least squares regression between EOS_a (also EOS_p) and the four climatic factors, and assigned the coefficient of temperature as the temperature sensitivity of EOS_a (γ_a) and for EOS_p (γ_b). The coefficient was commonly used as a proxy of changes in phenological dates per unit increase in temperature (i.e., temperature sensitivity)[49–51].

Separation of the effects of $NDVI_{max}$ in ΔNDVI and EOS_a. In this study, ΔNDVI for each month of senescence is also expressed as:

$$\Delta\mathrm{NDVI} = \delta\mathrm{NDVI} \times \mathrm{NDVI}_{\max} \quad (1)$$

This formula inherently indicates that ΔNDVI is jointly determined by δNDVI and $NDVI_{max}$. Trends of ΔNDVI during 1982–2018, therefore, can be separated into the trends of δNDVI and $NDVI_{max}$ based on the multiplication derivation rule ((uv)'=u'v + v'u, u and v are variables). The following approximation was used:

$$\mathrm{tr}[\Delta\mathrm{NDVI}] \approx \mathrm{tr}[\delta\mathrm{NDVI}] \times \mathrm{mean}[\mathrm{NDVImax}] + \mathrm{tr}[\mathrm{NDVImax}] \times \mathrm{mean}[\delta\mathrm{NDVI}] \quad (2)$$

where tr[ΔNDVI], tr[δNDVI] and tr[$NDVI_{max}$] are trends of ΔNDVI, δNDVI and $NDVI_{max}$ during the period 1982–2018, respectively. mean[$NDVI_{max}$] and mean[δNDVI] are the multi-year averages of $NDVI_{max}$ and δNDVI. tr[δNDVI] x mean[$NDVI_{max}$] and tr[$NDVI_{max}$] x mean[δNDVI] thus denote the contribution of δNDVI trends and $NDVI_{max}$ trends to ΔNDVI trends, respectively. To test the reliability of such approximation, we additionally checked whether the sum of the terms on the right-hand side of Eq. 2 (i.e., the partitioning approach) is equivalent to the left-hand side. The feasibility of such partitioning is ensured by a perfect 1:1 distribution of values on both side of Eq. 2 (Supplementary Fig. 16).

As for the EOS, once the thresholds of NDVI(T) and NDVI(T)/$NDVI_{max}$ were defined from the multi-year averaged NDVI curve (i.e., step 1 to step 4; Supplementary Fig. 12) the determination of EOS_a and EOS_p for each year (step 5, based on the prescribed thresholds) is less likely to be influenced by the peak times or decrease speed of NDVI. For example, if $NDVI_{max}$ keeps constant (e.g., 0.8), NDVI(T) for EOS_a is 0.2 and the NDVI(T)/$NDVI_{max}$ for EOS_p is 25%. No matter how the peak time and decrease speed changes, the time when NDVI value decrease to 0.2 always coincides with the time when a relative decrease to 25% occurred (Supplementary Fig. 17). Therefore, we can conclude that if $NDVI_{max}$ stays the same, EOS_a and EOS_p should be equal. Difference in EOS_a and EOS_p can thus be used to indicate asynchronization of EOS resulted from the increasing $NDVI_{max}$.

Data availability

All observational data sets that we used are publicly available. The GIMMS3g NDVI data sets covering the period 1982–2015 are publicly available at https://data.tpdc.ac.cn/en/data/9775f2b4-7370-4e5e-a537-3482c9a83d88/, datafiles covering the period 2016–2018 were directly requested from J. Tucker, the creator of GIMMS NDVI3g dataset. The CRU.TS.4.05 mean 2-m surface temperature data sets are available at https://data.ceda.ac.uk/badc/cru/data/cru_ts/cru_ts_4.05. The CRU.JRA v2.2 6-h insolation data sets are available at https://data.ceda.ac.uk/badc/cru/data/cru_jra/cru_jra_2.2. The C3S soil moisture data sets are available at https://cds.climate.copernicus.eu/cdsapp#!/dataset/satellite-soil-moisture?tab=overview. The ERA5 reanalysis wind speed data sets are available at https://cds.climate.copernicus.eu/cdsapp#!/dataset/reanalysis-era5-single-levels-monthly-means?tab=overview.

Code availability

All the analyses and figures are made using MATLAB R2020a and Power Point 2019, and the codes are available from the corresponding author.

Received: 24 November 2022; Accepted: 5 May 2023;
Published online: 19 May 2023

References

1. Piao, S. et al. Plant phenology and global climate change: Current progresses and challenges. *Glob Change Biol* **25**, 1922–1940 (2019).
2. Piao, S. et al. Net carbon dioxide losses of northern ecosystems in response to autumn warming. *Nature* **451**, 49–52 (2008).
3. Gallinat, A. S., Primack, R. B. & Wagner, D. L. Autumn, the neglected season in climate change research. *Trends Ecol Evol* **30**, 169–176 (2015).
4. Chen, L. et al. Leaf senescence exhibits stronger climatic responses during warm than during cold autumns. *Nat Clim Chang* **10**, 777–780 (2020).
5. Wang, X., Wu, C., Liu, Y., Peñuelas, J. & Peng, J. Earlier leaf senescence dates are constrained by soil moisture. *Glob Change Biol* **29**, 1557–1573 (2022).
6. Liu, Q. et al. Delayed autumn phenology in the Northern Hemisphere is related to change in both climate and spring phenology. *Glob Change Biol* **22**, 3702–3711 (2016).
7. Wu, C. et al. Widespread decline in winds delayed autumn foliar senescence over high latitudes. *Proceedings of the National Academy of Sciences* **118**, https://doi.org/10.1073/pnas.2015821118 (2021).
8. Wu, C. et al. Increased drought effects on the phenology of autumn leaf senescence. *Nat Clim Chang* **12**, 943–949 (2022).
9. Yu, H., Zhou, G., Lv, X., He, Q. & Zhou, M. Environmental factors rather than productivity drive autumn leaf senescence: evidence from a grassland in situ simulation experiment. *Agric For Meteorol* **327**, https://doi.org/10.1016/j.agrformet.2022.109221 (2022).
10. Estiarte, M. & Peñuelas, J. Alteration of the phenology of leaf senescence and fall in winter deciduous species by climate change: effects on nutrient proficiency. *Glob Change Biol* **21**, 1005–1017 (2015).
11. Keskitalo, J., Bergquist, G., Gardeström, P. & Jansson, S. A Cellular Timetable of Autumn Senescence. *Plant Physiol* **139**, 1635–1648 (2005).
12. Lim, P. O., Kim, H. J. & Gil Nam, H. Leaf Senescence. *Annu Rev Plant Biol* **58**, 115–136 (2007).
13. Deslauriers, A., Rossi, S. & Sevanto, S. Metabolic memory in the phenological events of plants: looking beyond climatic factors. *Tree Physiol* **39**, 1272–1276 (2019).
14. Fracheboud, Y. et al. The Control of Autumn Senescence in European Aspen. *Plant Physiol* **149**, 1982–1991 (2009).
15. Piao, S., Wang, J., Li, X., Xu, H. & Zhang, Y. Spatio-temporal changes in the speed of canopy development and senescence in temperate China. *Glob Change Biol* **28**, 7366–7375 (2022).
16. Vitasse, Y., Bresson, C. C., Kremer, A., Michalet, R. & Delzon, S. Quantifying phenological plasticity to temperature in two temperate tree species. *Funct Ecol* **24**, 1211–1218 (2010).
17. Anav, A. et al. Evaluation of Land Surface Models in Reproducing Satellite Derived Leaf Area Index over the High-Latitude Northern Hemisphere. Part II: Earth System Models. *Remote Sens* **5**, 3637–3661 (2013).
18. Murray-Tortarolo, G. et al. Evaluation of Land Surface Models in Reproducing Satellite-Derived LAI over the High-Latitude Northern Hemisphere. Part I: Uncoupled DGVMs. *Remote Sens* **5**, 4819–4838 (2013).
19. Wu, Z. et al. Atmospheric brightening counteracts warming-induced delays in autumn phenology of temperate trees in Europe. *Glob Ecol Biogeogr* **30**, 2477–2487 (2021).
20. Zhang, Y., Commane, R., Zhou, S., Williams, A. P. & Gentine, P. Light limitation regulates the response of autumn terrestrial carbon uptake to warming. *Nat Clim Chang* **10**, 739–743 (2020).
21. Mainiero, R. & Kazda, M. Effects of Carex rostrata on soil oxygen in relation to soil moisture. *Plant Soil* **270**, 311–320 (2005).
22. Liu, H. et al. Phenological mismatches between above- and belowground plant responses to climate warming. *Nat Clim Chang* **12**, 97–102 (2021).
23. Leuzinger, S., Zotz, G., Asshoff, R. & Korner, C. Responses of deciduous forest trees to severe drought in Central Europe. *Tree Physiol* **25**, 641–650 (2005).
24. Lian, X. et al. Summer soil drying exacerbated by earlier spring greening of northern vegetation. *Sci Adv* **6**, https://doi.org/10.1126/sciadv.aax0255 (2020).
25. Zhang, Y., Keenan, T. F. & Zhou, S. Exacerbated drought impacts on global ecosystems due to structural overshoot. *Nat Ecol Evol* **5**, 1490–1498 (2021).
26. Dietze, M. C. et al. Nonstructural Carbon in Woody Plants. *Annu Rev Plant Biol* **65**, 667–687 (2014).
27. Fu, Y. S. H. et al. Variation in leaf flushing date influences autumnal senescence and next year's flushing date in two temperate tree species. *Proceedings of the National Academy of Sciences* **111**, 7355–7360 (2014).
28. Piao, S. et al. Characteristics, drivers and feedbacks of global greening. *Nat Rev Earth Environ* **1**, 14–27 (2019).
29. Zhu, Z. et al. Greening of the Earth and its drivers. *Nat Clim Chang* **6**, 791–795 (2016).
30. Richardson, A. D. et al. Terrestrial biosphere models need better representation of vegetation phenology: results from the North American Carbon Program Site Synthesis. *Glob Change Biol* **18**, 566–584 (2012).
31. Keenan, T. F. et al. Net carbon uptake has increased through warming-induced changes in temperate forest phenology. *Nat Clim Chang* **4**, 598–604 (2014).
32. Krinner, G. et al. A dynamic global vegetation model for studies of the coupled atmosphere-biosphere system. *Glob Biogeochem Cycle* **19**, https://doi.org/10.1029/2003GB002199 (2005).
33. Medvigy, D., Wofsy, S. C., Munger, J. W., Hollinger, D. Y. & Moorcroft, P. R. Mechanistic scaling of ecosystem function and dynamics in space and time: Ecosystem Demography model version 2. *J Geophys Res* **114**, https://doi.org/10.1029/2008JG000812 (2009).

34. Caffarra, A., Donnelly, A. & Chuine, I. Modelling the timing of Betula pubescens budburst. II. Integrating complex effects of photoperiod into process-based models. *Clim Res* **46**, 159–170 (2011).
35. Dufrêne, E. et al. Modelling carbon and water cycles in a beech forest. *Ecol Model* **185**, 407–436 (2005).
36. Jeong, S. J. & Medvigy, D. Macroscale prediction of autumn leaf coloration throughout the continental United States. *Glob Ecol Biogeogr* **23**, 1245–1254 (2014).
37. Tucker, C. J. et al. An extended AVHRR 8-km NDVI dataset compatible with MODIS and SPOT vegetation NDVI data. *Int J Remote Sens* **26**, 4485–4498 (2010).
38. Kaufmann, R. K. et al. Effect of orbital drift and sensor changes on the time series of AVHRR vegetation index data. *IEEE Trans Geosci Remote Sensing* **38**, 2584–2597 (2000).
39. Friedl, M. A. et al. MODIS Collection 5 global land cover: Algorithm refinements and characterization of new datasets. *Remote Sens Environ* **114**, 168–182 (2010).
40. Harris, I., Osborn, T. J., Jones, P. & Lister, D. Version 4 of the CRU TS monthly high-resolution gridded multivariate climate dataset. *Sci Data* **7**, https://doi.org/10.1038/s41597-020-0453-3 (2020).
41. Kobayashi, S. et al. The JRA-55 Reanalysis: General Specifications and Basic Characteristics. *Journal of the Meteorological Society of Japan Ser II* **93**, 5–48 (2015).
42. Bell, B. et al. The ERA5 global reanalysis: Preliminary extension to 1950. *Q J R Meteorol Soc* **147**, 4186–4227 (2021).
43. Piao, S., Fang, J., Zhou, L., Ciais, P. & Zhu, B. Variations in satellite-derived phenology in China's temperate vegetation. *Glob Change Biol* **12**, 672–685 (2006).
44. Jeong, S. J., Ho, C. H., Gim, H. J. & Brown, M. E. Phenology shifts at start vs. end of growing season in temperate vegetation over the Northern Hemisphere for the period 1982-2008. *Glob Change Biol* **17**, 2385–2399 (2011).
45. White, M. A. et al. Intercomparison, interpretation, and assessment of spring phenology in North America estimated from remote sensing for 1982-2006. *Glob Change Biol* **15**, 2335–2359 (2009).
46. Cong, N. et al. Changes in satellite-derived spring vegetation green-up date and its linkage to climate in China from 1982 to 2010: a multimethod analysis. *Glob Change Biol* **19**, 881–891 (2013).
47. Gill, A. L. et al. Changes in autumn senescence in northern hemisphere deciduous trees: a meta-analysis of autumn phenology studies. *Ann Bot* **116**, 875–888 (2015).
48. Liu, L. et al. Soil moisture dominates dryness stress on ecosystem production globally. *Nat Commun* **11**, https://doi.org/10.1038/s41467-020-18631-1 (2020).
49. Fu, Y. H. et al. Declining global warming effects on the phenology of spring leaf unfolding. *Nature* **526**, 104–107 (2015).
50. Menzel, A. et al. European phenological response to climate change matches the warming pattern. *Glob Change Biol* **12**, 1969–1976 (2006).
51. Yang, Y., Guan, H., Shen, M., Liang, W. & Jiang, L. Changes in autumn vegetation dormancy onset date and the climate controls across temperate ecosystems in China from 1982 to 2010. *Glob Change Biol* **21**, 652–665 (2015).

Acknowledgements

This study was supported by the National Natural Science Foundation of China (41988101).

Author contributions

S.L.P., Y.C.Z., S.B.H. and Q.L. designed the research; Y.C.Z. performed analysis; Y.C.Z. wrote the first draft of the manuscript. C.H., J.P., S.R. and R.B.M. contributed to the interpretation of the results and to the text.

Competing interests

The authors declare no competing interests.

Additional information

Supplementary information The online version contains supplementary material available at https://doi.org/10.1038/s43247-023-00835-0.

Correspondence and requests for materials should be addressed to Qiang Liu or Shilong Piao.

Peer review information *Communications Earth & Environment* thanks the anonymous reviewers for their contribution to the peer review of this work. Primary Handling Editor: Aliénor Lavergne.